

Electron Paramagnetic and Nuclear Double Resonance of F^+ Centers in BeO Single Crystals

R. C. DUVARNEY, A. K. GARRISON, AND R. H. THORLAND
Physics Department, Emory University, Atlanta, Georgia 30322
 (Received 9 June 1969)

Single crystals of BeO which have been irradiated with neutrons show an EPR spectrum with partially resolved hyperfine structure. An ENDOR study of the hyperfine interaction leads to the conclusion that the spectrum arises from centers which consist of an electron trapped at an oxygen vacancy surrounded by four Be nuclei. The measured hyperfine interaction constants are: $A_{\perp}/h = 10.3$ MHz, $A_{\parallel}/h = 16.4$ MHz, and $(e^2gQ)/h = 1.1$ MHz for the Be nuclei not on the c axis; and $A_{\perp}/h = 4.2$ MHz, $A_{\parallel}/h = 9.2$ MHz, and $(e^2gQ)/h = 1.5$ MHz for the nuclei along the c axis. These values lead to $|\psi(\mathbf{r}_{\text{Be}})|^2 = 0.13 \times 10^{24}$ cm $^{-3}$ for the electron wave function at the c -axis nuclei, and $|\psi(\mathbf{r}_{\text{Be}})|^2 = 0.06 \times 10^{24}$ cm $^{-3}$ for the nonaxial nuclei. The measured g value for \mathbf{H} parallel to the c axis is 2.0030.

INTRODUCTION

ELECTRON-PARAMAGNETIC-RESONANCE (EPR) and electron-double-nuclear-resonance (ENDOR) experiments have established a microscopic model for the F^+ center in some cubic alkaline-earth oxide crystals. Those reported in the literature are MgO,^{1,2} CaO,^{3,4} and SrO.⁵ The model supported by these experiments is an electron trapped at an anion vacancy, which is the same as the de Boer⁶ model for the F center in the alkali halides. We have chosen to call this one-electron center in divalent crystals an F^+ center, as has been suggested in the recent review article by Henderson and Wertz.⁷

BeO is the lightest alkaline-earth oxide and has a hexagonal wurtzite crystal structure consisting of interlocking O and Be tetrahedra. Although it has a different crystal structure from the other alkaline-earth oxides, a complete study of the F^+ center in this series should also include BeO. Some previous EPR work on neutron-irradiated polycrystalline samples has been reported by Troup and Thyer.⁸ They report an EPR line with $g_{\parallel} = 2.0036$ and $g_{\perp} = 2.0110$ and an over-all linewidth of 30 G, although the change of line shape upon annealing leads them to conclude that the line may come from more than one kind of center.

In this paper, the results of an EPR-ENDOR experiment on single crystals of BeO which have been irradiated with neutrons are described. The neutron-irradiated crystals show an EPR hyperfine pattern which has been previously reported and which was tentatively interpreted as arising from F^+ centers,

although a complete analysis could not be made because of the lack of resolution of the hfs at arbitrary orientations of the crystal.⁹ An ENDOR experiment seemed appropriate and the BeO system turned out to be particularly straightforward for this kind of experiment. The ENDOR results presented here confirm the earlier EPR interpretation. In addition, they give more accurate values for the magnetic hyperfine coupling constants and new values for the electric quadrupole coupling constants for the F^+ -center electron and the surrounding nearest-neighbor (nn) beryllium nuclei.

Another unique feature of these results is that they quite clearly show the effect of the relative shift of the interlocking Be and O tetrahedron along the c axis. These conditions make the crystal pyroelectric, and hence there is a large electric field along the c axis. The measured hyperfine coupling constants of the F^+ -center electron reflect this by the fact that the coupling with the Be nucleus along the c axis differs from the coupling with the other three Be nuclei.

EXPERIMENTAL

The BeO single crystals that were used in this study were supplied by Newkirk of the Lawrence Radiation Laboratory. In appearance the crystals were transparent and colorless and from 10 to 50 mm³ in volume. The [0001] or c axis of this wurtzite-type structure was parallel to the longest dimension of the crystals

TABLE I. Impurity content of BeO crystals used in this study.

Impurity	Concentration (atomic ppm)
Al	100
Ca	7
Cr	1
Mg	4
Si	64
Mo, Li	<15

¹ J. E. Wertz, P. Auzins, R. A. Weeks, and R. H. Silsbee, *Phys. Rev.* **107**, 1535 (1957).

² W. P. Unruh and J. W. Culvahouse, *Phys. Rev.* **154**, 861 (1967).

³ J. C. Kemp and V. I. Neely, *J. Phys. Chem. Solids* **24**, 332 (1963).

⁴ T. Chang, T. C. Ensign, and B. Henderson, *Bull. Am. Phys. Soc.* **13**, 1415 (1968).

⁵ J. W. Culvahouse, L. V. Holroyd, and J. L. Kolopus, *Phys. Rev.* **140**, A1181 (1965).

⁶ J. H. de Boer, *Rec. Trav. Chim.* **56**, 301 (1937).

⁷ B. Henderson and J. E. Wertz, *Advan. Phys.* **17**, 749 (1968).

⁸ G. J. Troup and J. R. W. Thyer, *Proc. Phys. Soc. (London)* **79**, 409 (1962).

⁹ R. H. Thorland and A. K. Garrison, *Bull. Am. Phys. Soc.* **13**, 1699 (1968).

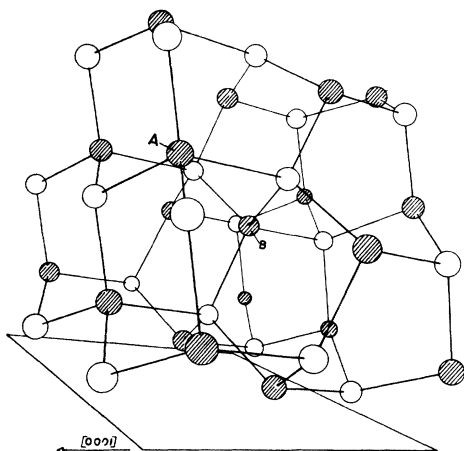


FIG. 1. Wurtzite crystal structure of BeO. The shaded circles represent oxygen ions and the unshaded circles represent Be ions. The sites labeled A and B show the two possible kinds of sites for F^+ centers. The crystal structure rests on a $\{0110\}$ plane.

as indicated by the hexagonal cross section of the crystals in a plane perpendicular to this long dimension. The impurity content of the samples is given in Table I.¹⁰

The samples were irradiated with neutrons of energy greater than 1 MeV to a total dose of $5.4 \times 10^{18}/\text{cm}^2$ at a temperature of about 38°C. The irradiations were done at the Oak Ridge Research Reactor of the Oak Ridge National Laboratory. Samples so treated acquired a yellow-amber coloration and were subsequently kept in a dark environment to prevent bleaching of the EPR signal. This precaution, however, proved to be unnecessary.

The ESR studies were done on a Varian V-4500, X-band spectrometer equipped with 100-kHz field modulation and phase-sensitive detection. Also employed was a Varian V-4531 rectangular cavity operating in the TE_{012} mode and a Varian 9-in. electromagnet with a Fieldial Mark-I power supply. Accurate measurements of the magnetic field were made with an Alpha Scientific Laboratories proton probe and a Hewlett-Packard 5246L frequency counter. This counter, in conjunction with a Hewlett-Packard 5255A frequency converter, was also used to measure the klystron frequency.

The samples were introduced into the microwave cavity on one end of a quartz rod. The other end was fixed to a goniometer which allowed the orientation of the crystal to be changed with respect to the external magnetic field. Two quartz rods were used. Each rod had the end which was used to mount the sample cut at that angle which, under crystal rotation, keeps the external magnetic field in the (0001) and (0110) crystalline planes, respectively.

The ENDOR studies were performed with a slightly modified version of the previously described spectrom-

eter. A five-turn coil of number-24 enameled copper wire was introduced into the rectangular TE_{012} cavity. The coil, rectangular in shape, was located in a plane perpendicular to the long dimension of the cavity and midway between the cavity walls. The narrow dimension of the coil was semicircular to allow clearance for the sample to be introduced into the cavity. This arrangement proved to be quite satisfactory in that it lowered the Q of the system only slightly and yet allowed the efficient production of large radio-frequency fields of the proper geometry at the sample position.

This coil was driven with a radio-frequency oscillator of the push-pull type¹¹ using a high-power double pentode (829-B). The design employed a set of plug-in inductors which gave a continuous tuning range from 2 to 20 MHz. This oscillator supplied sufficient power to the coil to generate a radio-frequency field whose magnetic component, measured at the sample position, was 20 G peak-to-peak.

The sample was introduced into the cavity on the end of a copper cold finger. The cold finger is attached to the base of a liquid-nitrogen cryostat and is shielded with a Vycor glass tube. It should be noted that although the ENDOR study was done at 77°K, it is not mandatory to operate at low temperature. The ENDOR signal can be observed in this system at room temperature with an intensity reduction of about a factor of 3 from the low-temperature spectrum. The orientation of the sample in the external magnetic field was varied by rotating the entire cryostat assembly.

The ENDOR data were taken using the following phase-sensitive technique. The ESR spectrum is first recorded on the spectrometer employing 100-kHz magnetic field modulation and phase-sensitive detection. The magnetic field is then set at a suitable location within the spectrum; the 100-kHz field modulation is left on and the microwave power is increased in order to partially saturate the absorption spectrum. The radio-frequency oscillator is then swept over its tuning range using a clock motor drive, and the resulting changes in the level of saturation of the sample are recorded as a function of frequency as measured on the frequency counter. Although this is a relatively unsophisticated technique, the results were quite acceptable in that the ENDOR signal-to-noise ratio was of the order of 50:1 (to be shown in Fig. 3).

RESULTS

In order to present the EPR and ENDOR results, it is useful to consider first in some detail the crystal structure of BeO and its relation to the hyperfine interaction. As will be shown below, the angular dependence of the hyperfine interaction can be related to the O-Be bond directions, hence these are the essential geometrical elements in the results and their

¹⁰ H. Newkirk (private communication).

¹¹ Circuit diagram supplied by C. L. Marquardt and F. W. Patten.

analysis. Figure 1 represents the wurtzite crystal lattice structure of BeO and shows the two possible inequivalent anion-vacancy sites marked *A* and *B*. In each site, the trapped electron is surrounded by four Be nuclei at the corners of a tetrahedron, but the tetrahedra at each site differ by a 60° rotation about the *c* axis. In the undamaged crystal, the Be-O bond length along the *c* axis is 1.655 Å and is 1.647 Å along the other three directions.¹² The bond angles with the *c* axis are 109.0° and the other three Be-O-Be angles are 110.0°.¹²

From a consideration of the bond directions at sites *A* and *B* as represented in Fig. 1, one can make the following general statements about the angular dependence of the hyperfine interaction of a trapped electron at *A* or *B*: (1) The two sites give the same hyperfine interaction when the magnetic field (**H**) is parallel to the *c* axis; (2) for rotation of **H** in a {0110} plane the two sites, *A* and *B*, are equivalent and there are four different angular variations from each of the four nuclei at each site; (3) rotation of **H** in a {1210} plane gives five different angular variations, since there are two equivalent nuclei at each site and the angular variation from the nucleus along the *c* axis is the same for each site.

The EPR spectrum for the magnetic field parallel to the *c* axis is shown in Fig. 2(a). It consists of 13 lines with a spacing of about 4 G. This is the kind of hyperfine pattern one might expect from a hyperfine interaction with four nearly equivalent nuclei with $\frac{3}{2}$ spin. The large line at the low-field end of the spectrum is due to another radiation-induced paramagnetic center that has not been identified. The 13-line spectrum

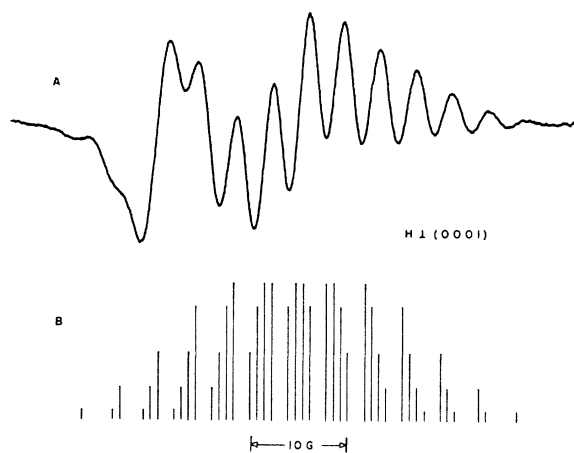


FIG. 2. Comparison of EPR spectrum with calculated stick diagram. (a) The EPR spectrum showing the derivative of the absorption versus magnetic field. The large line at the left end of the hyperfine pattern is due to another center. (b) A stick diagram showing the position of the EPR absorption lines for **H**||*c* constructed from the magnetic hyperfine constants measured by ENDOR. The 10-G scale applies to both parts *A* and *B*.

¹² G. A. Jeffrey, G. S. Parry, and R. L. Mozzi, *J. Chem. Phys.* **25**, 1024 (1956).

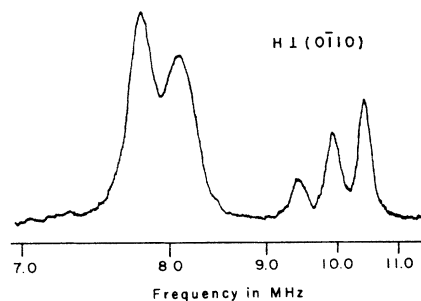


FIG. 3. ENDOR spectrum showing the change of the saturation level versus the frequency of the ENDOR oscillator. This spectrum is for the five data points at 90° on the graph of Fig. 5.

saturates easily at room temperature so that the EPR data were taken at 30–40 dB attenuation of 150 mW of klystron power incident on the cavity. Rotation of the magnetic field to an arbitrary direction in the crystal gave EPR spectra that were much poorer in resolution, though the over-all width of the spectrum was about the same for that shown in Fig. 2(a).

The *g* value was measured to be 2.0030 at **H** parallel to the *c* axis. The values appeared to be isotropic, but a complete confirmation of this was made difficult by the poor resolution and interference from other lines.

The partial resolution of the EPR signal greatly facilitated the search for the ENDOR lines, since an approximate value of the hyperfine coupling constants was known. Both pair of ENDOR patterns corresponding to nuclear transitions within the electron spin-up ($m_s = \frac{1}{2}$) and spin-down ($m_s = -\frac{1}{2}$) energy levels were observed. However, the pattern for spin down had a lower intensity by a factor of 10 and thus the angular dependence studies were made only on the spin-up pattern. Figure 3 shows a typical ENDOR spectrum for the spin-up pattern.

The ENDOR data are shown in Figs. 4 and 5. The dots show the experimental points and the solid lines the calculated values. Figure 4 shows the angular variation for rotation about a {0110} axis and Fig. 5 is for a rotation about a {1210} axis. The angle is between the magnetic field and the *c* axis. In Fig. 4 there are four groups of three lines and each group is associated with one of the four Be nuclei surrounding the trapped electron. There are only four in this case as explained in the discussion of symmetry above. Note that at **H** parallel to the *c* axis the interaction of all four nuclei is almost the same and hence the ENDOR data very clearly indicate how one gets the 13-line hyperfine pattern in the EPR data. The group of three lines that decreases in frequency is associated with the nuclei along the *c* axis. Figure 5 shows five groups of lines which arise from the symmetry as explained above. Data were not taken for the *c*-axis nuclei in this case because it was a repeat of that shown in Fig. 4. The lack of a very close fit at 90° for the central groups is due to a slight misalignment of the crystal, which is estimated to be less than a degree.

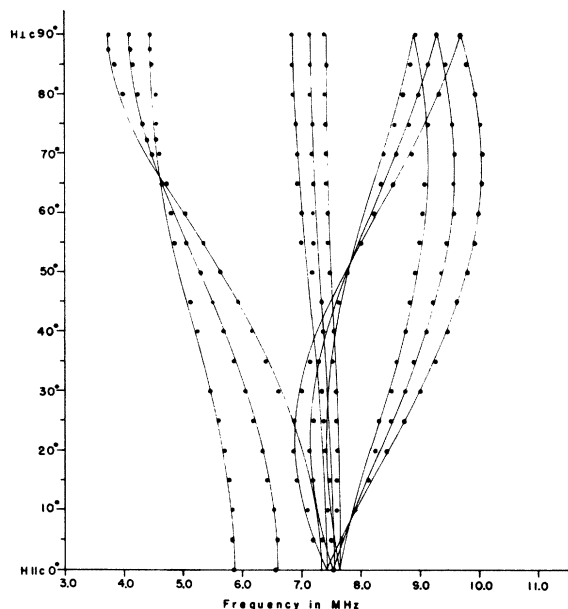


FIG. 4. Graph showing the frequency of the ENDOR lines versus the angle the magnetic field makes with the c axis for rotation about a (0110) axis. The dots give the experimental points and the solid lines the calculated values.

In Figs. 4 and 5, the splitting of each group of lines into three is due to the electric quadrupole interaction which was easily resolved at most angles.

The ENDOR data were analyzed using a Hamiltonian for one Be nucleus of the form

$$\mathcal{H}C = g\beta H_z S_z + |\gamma_{Be}| \hbar H_z I_z + \mathbf{I} \cdot \mathbf{A} \cdot \mathbf{S} + [e^2 Q q / 4I(2I-1)](3I_z^2 - I^2), \quad (1)$$

where β is the Bohr magneton, γ_{Be} is the gyromagnetic ratio of the Be nucleus, H_z is the z component of the magnetic field \mathbf{H} , I is the nuclear spin, S is the electron spin, \mathbf{A} is the hyperfine interaction tensor, e is the electron charge, Q is the nuclear quadrupole moment, and q is the z' principal element of the electric-field-gradient tensor. The unprimed axis system has a z axis fixed with the magnetic field and a y axis as the axis of rotation of the crystal and the primed axis system is the principal axis system of the magnetic and electric quadrupole interaction tensors. In the analysis, the z' axis was taken along the bond directions. The data could be fitted within experimental accuracy by assuming axial hyperfine tensors.

Using the above Hamiltonian, assuming that the electron spin is quantized along the external field direction and that the nuclear spin is quantized along the effective field,¹³ one obtains an expression for the ENDOR frequencies of the form

$$\nu = (\nu_L^2 + 2\nu_L a_1 m_S + a_2 m_S^2)^{1/2} + (e^2 q Q / 4\hbar)(3\alpha_{z'z_{\text{eff}}}^2 - 1)(m_I + \frac{1}{2}), \quad (2)$$

¹³ C. P. Slichter, *Principles of Magnetic Resonance* (Harper & Row Publishers, Inc., New York, 1963), p. 195.

where

$$a_1 = (A_1/\hbar)(1 - \alpha_{zz'})^2 + (A_{11}/\hbar)\alpha_{zz'}^2, \quad (3)$$

$$a_2 = (A_1/\hbar)^2(1 - \alpha_{zz'}^2) + (A_{11}/\hbar)^2\alpha_{zz'}^2. \quad (4)$$

In these expressions ν_L is the Larmor frequency of the Be nucleus; $\alpha_{zz'}$ is the direction cosine of the z axis of the primed system with respect to the z axis of the unprimed system (direction cosine of the magnetic field with respect to a bond direction); $\alpha_{z'z_{\text{eff}}}$ is the direction cosine of the effective magnetic field with respect to the z' axis (bond direction); m_S specifies the electron-spin energy level within which the ENDOR transitions take place and has the values $\pm\frac{1}{2}$; m_I specifies the lower level of the $\Delta m_I = 1$ nuclear transitions and has the value $-\frac{3}{2}$, $-\frac{1}{2}$, and $\frac{1}{2}$. In obtaining this expression, the terms in (S_x') , (S_y') , $(I_x'I_y')$, $(I_x'I_z')$, and $(I_x'I_x')$ of Eq. (1) were neglected.

The experimental data clearly show that the applied magnetic field and the effective magnetic field are not the same. This is evident from the data in Fig. 4 showing the quadrupole splitting for the nuclei along the c axis going to zero at about 65° . If the nuclear spin were quantized along the applied field, then the collapse of the quadrupole splitting should occur at about 55° for these particular nuclei. The zero quadrupole splitting for the other two groups of lines in Fig. 4 occurs at different angles because the angle read off the graph is not the angle with the bond for these nuclei.

One can see from Eqs. (2)–(4) that when the magnetic field is along a principal axis the difference in the

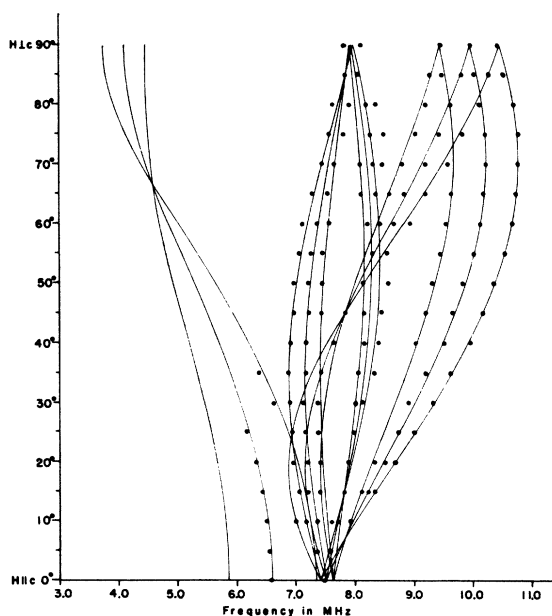


FIG. 5. Graph showing the frequency of the ENDOR lines versus the angle the magnetic field makes with the c axis for rotation about a (1210) axis. The dots give the experimental points and the solid lines the calculated values.

TABLE II. Hyperfine coupling constants and electron density at Be nuclei for F^+ center in BeO.

Nucleus	(A_{\perp}/h) (MHz)	(A_{\parallel}/h) (MHz)	$(e^2Qq)/h$ (MHz)	$a = \frac{1}{3}(2A_{\perp} + A_{\parallel})$ (MHz)	$b = \frac{1}{3}(A_{\parallel} - A_{\perp})$ (MHz)	$ \psi(\mathbf{r}_{Be}) ^2$ (cm^{-3})
Basal nn Be	10.3	16.4	1.1	12.3	2.0	0.13×10^{24}
c -axis nn Be	4.2	9.2	1.5	5.8	1.7	0.06×10^{24}

ENDOR frequency of the $m_s = \frac{1}{2}$ and the $m_s = -\frac{1}{2}$ states is twice the Larmor frequency when the hyperfine interaction energy is greater than the nuclear Zeeman energy. But when the nuclear Zeeman energy is greater than the hyperfine interaction, the frequency gives the hyperfine constant. In the case of BeO, the former condition was met so that the Larmor frequency could be computed from the measured frequency difference and used to verify that the interaction was from Be nuclei. The values of the magnetic and electric quadrupole hyperfine coupling constants were obtained from the data when the external magnetic field was perpendicular and parallel to the various bond directions. This resulted in the same values for all the nuclei not along the c axis (basal nuclei) and another value for the nuclei along the c axis (axial nuclei). These values are given in Table II. The solid lines on Figs. 3 and 4 were calculated from the values in Table II using Eqs. (2)–(4) and the known bond directions. Figure 2(b) shows a stick diagram of the EPR spectrum for the magnetic field parallel to the c axis constructed from the magnetic hyperfine coupling constants obtained from the ENDOR data. It shows how the clearly resolved EPR pattern of Fig. 2(a) results.

Attempts to correlate the F^+ -center EPR-ENDOR spectra with the expected optical-absorption band have not yet met with success. The absorption spectrum of the unirradiated crystals was flat from 700 to 200 nm. The colored specimens used in the EPR-ENDOR experiments had an absorption spectrum showing increasing absorption from 700 nm with a shoulder at 340 nm, and well-defined peaks at 303 nm and at 230 nm. These heavily irradiated specimens were quite opaque below 270 nm, so that the higher-energy bands were taken after one of the crystals was cut to a thickness of about 0.1 mm. No observations were made below 210 nm and all observations were made at room temperature. Irradiation of the colored crystals at 77°K with a broad spectrum of visible and ultraviolet light from a mercury lamp produced no effect on the F^+ -center EPR spectrum.

CONCLUSION

The results presented in the previous section support the conclusion that the center responsible for the EPR-ENDOR spectra reported here is a single elec-

tron trapped at an oxygen vacancy to form what is called an F^+ center. The ENDOR results show that the hyperfine interaction is with the four nearest-neighbor Be nuclei, which is the crucial evidence supporting the model. The paramagnetic state of O ions, namely, O^- or O^{--} , would probably be found at an interstitial position and would not show the symmetry of the observed data. It would also seem that x irradiation might produce a valence change in the O ions to make them paramagnetic whereas only neutron irradiation produces the observed resonance. Other possible impurities such as B, Al, Si, Li, and F have nuclear spins which would give different ENDOR results. The g value reported here is consistent with the value for the center reported by Troup and Thyer.⁷

Some details of the model can readily be deduced from the ENDOR results, but their interpretation is somewhat involved and shall be discussed elsewhere. The magnetic hyperfine coupling constant given in Table II can be used to compute the electron density at the surrounding Be nuclei by using the expression for the isotropic coupling constant

$$a = (16/3)\pi\beta\gamma_{Be}\hbar|\psi(\mathbf{r}_{Be})|^2.$$

The values for $|\psi(\mathbf{r}_{Be})|^2$ are smaller than the value for $|\psi(\mathbf{r}_{Mg})|^2$ for the F^+ center in MgO,¹ which seems to indicate that the F^+ -center electron in BeO is more tightly bound. It should also be noted that although the electron density is smaller for the c -axis Be than for basal Be, the gradient of the electric field is larger. An interpretation of the effect of lattice distortion and crystal electric field on the electric field gradient will be made after further studies of the effect of temperature variation on the size of the quadrupole coupling constants. Further work is also in progress to identify the F^+ -center optical bands.

ACKNOWLEDGMENTS

The authors wish to thank Dr. Herbert Newkirk for kindly supplying the crystals and information on them, and Dr. James L. Kolopus for his invaluable assistance with the neutron irradiations. The construction of the cryostat and other apparatus by O. H. Puckett was particularly beneficial. Robert Burnett helped with the optical measurements. We acknowledge helpful discussions with Dr. Frank Pattern and C. L. Marquardt.